JOURNAL OF GEOPHYSICAL RESEARCH: ATMOSPHERES, VOL. 118, 4801–4815, doi:10.1002/jgrd.50449, 2013

Estimating the direct radiative effect of absorbing aerosols overlying marine boundary layer clouds in the southeast Atlantic using MODIS and CALIOP

Kerry Meyer,[1,2] Steven Platnick,[2] Lazaros Oreopoulos,[2] and Dongmin Lee[1,2]

Received 26 October 2012; revised 17 April 2013; accepted 24 April 2013; published 29 May 2013.

[1] Absorbing aerosols such as smoke strongly absorb solar radiation, particularly at ultraviolet and visible/near-infrared (VIS/NIR) wavelengths, and their presence above clouds can have considerable implications. It has been previously shown that they have a positive (i.e., warming) direct aerosol radiative effect (DARE) when overlying bright clouds. Additionally, they can cause biased passive instrument satellite retrievals in techniques that rely on VIS/NIR wavelengths for inferring the cloud optical thickness (COT) and effective radius (r_e) of underlying clouds, which can in turn yield biased above-cloud DARE estimates. Here we investigate Moderate Resolution Imaging Spectroradiometer (MODIS) cloud optical property retrieval biases due to overlying absorbing aerosols observed by Cloud-Aerosol Lidar with Orthogonal Polarization (CALIOP) and examine the impact of these biases on above-cloud DARE estimates. The investigation focuses on a region in the southeast Atlantic Ocean during August and September (2006–2011), where smoke from biomass burning in southern Africa overlies persistent marine boundary layer stratocumulus clouds. Adjusting for above-cloud aerosol attenuation yields increases in the regional mean liquid COT (averaged over all ocean-only liquid clouds) by roughly 6%; mean r_e increases by roughly 2.6%, almost exclusively due to the COT adjustment in the non-orthogonal retrieval space. It is found that these two biases lead to an underestimate of DARE. For liquid cloud Aqua MODIS pixels with CALIOP-observed above-cloud smoke, the regional mean above-cloud radiative forcing efficiency (DARE per unit aerosol optical depth (AOD)) at time of observation (near local noon for Aqua overpass) increases from 50.9Wm^{-2}AOD^{-1} to 65.1Wm^{-2}AOD^{-1} when using bias-adjusted instead of nonadjusted MODIS cloud retrievals.

Citation: Meyer, K., S. Platnick, L. Oreopoulos, and D. Lee (2013), Estimating the direct radiative effect of absorbing aerosols overlying marine boundary layer clouds in the southeast Atlantic using MODIS and CALIOP, *J. Geophys. Res. Atmos.*, *118*, 4801–4815, doi:10.1002/jgrd.50449.

1. Introduction

[2] Significant efforts have been undertaken in recent years to characterize aerosol optical and microphysical properties and to quantify their direct and indirect radiative effects, as they remain a poorly constrained component of the Earth's atmosphere [*Forster et al.*, 2007]. One region that has received substantial attention is the southeast Atlantic Ocean, off the southwestern coast of Africa. Each year during austral winter, extensive biomass burning occurs throughout southern Africa, injecting large amounts of smoke into the troposphere: For the years 1997–2009, the portion of Africa south of the equator was estimated to contribute roughly 28% of global biomass burning carbon emissions, with emission rates during the burning season peaking annually between 100 and 150 Tg month^{-1} [*van der Werf et al.*, 2010]. Prevailing easterly winds frequently transport this smoke westward off the continent, creating a near-persistent smoke layer over the southeastern Atlantic Ocean. The concurrent meteorological conditions over this region of the Atlantic are such that widespread, near-persistent marine boundary layer (MBL) stratocumulus clouds are also present. A unique situation is thus created as the smoke layer, originating inland at higher altitudes, overlies the low-altitude MBL clouds [*Devasthale and Thomas*, 2011] with considerable implications. First, the microphysical and macrophysical properties of the MBL clouds can be altered if cloud top entrainment couples an overlying aerosol layer, affecting cloud albedo (first indirect effect) [*Twomey*, 1974, 1977a] and potentially also cloud lifetime (second indirect effect) [*Albrecht*, 1989], or via changes in the above-cloud thermodynamic conditions because of aerosol absorption (semi-indirect effect) [*Ackerman et al.*, 2004].

[1]Goddard Earth Sciences Technology and Research (GESTAR), Universities Space Research Association, Columbia, MD, USA.
[2]NASA Goddard Space Flight Center, Greenbelt, Maryland, USA.

Corresponding author: K. Meyer, NASA Goddard Space Flight Center, Code 613.0, Greenbelt, MD 20771, USA. (kerry.meyer@nasa.gov)

2169-897X/13/10.1002/jgrd.50449

[3] Second, smoke aerosols, composed primarily of carbonaceous particles, strongly absorb solar radiation, particularly at ultraviolet (UV) and visible (VIS) wavelengths [*Bond and Bergstrom*, 2006]. Several recent studies have provided estimates of this direct aerosol radiative effect (DARE) above clouds over the southeastern Atlantic Ocean. For instance, *Chand et al*. [2009] estimated above-cloud diurnal DARE by initializing forward radiative transfer (RT) calculations with monthly mean aerosol optical properties derived from the color ratio technique [*Chand et al*., 2008] developed for CALIOP (Cloud-Aerosol Lidar with Orthogonal Polarization), on board CALIPSO (Cloud-Aerosol Lidar and Infrared Pathfinder Satellite Observation) [*Winker et al*., 2009], and monthly mean cloud properties from the Moderate Resolution Imaging Spectroradiometer (MODIS) on board NASA's Terra satellite. They found that smoke aerosols have a net warming effect when the underlying cloud fraction was 0.4 or greater, and that the warming effect increases approximately linearly with cloud fraction (mean diurnal direct radiative effect during July–October 2006/2007 approaches roughly 12 to 14Wm^{-2} off the coast of Namibia).

[4] *Wilcox* [2011], using a more indirect approach, estimated above-cloud aerosol radiative effect by investigating the relationship between cloud albedo and cloud liquid water path as a function of above-cloud aerosol loading. Cloud albedo was obtained from CERES (Clouds and Earth's Radiant Energy System) and liquid water path from AMSR-E (Advanced Microwave Scanning Radiometer for EOS); aerosol loading was estimated using the OMI (Ozone Monitoring Instrument) UV aerosol index (UVAI). Over the southeast Atlantic Ocean (10°W to 15°E longitude, 20°S to 0°S latitude) during austral winter (July to September of 2005 and 2006), the direct and semidirect (due to cloud layer thickening) aerosol radiative effect for overcast scenes with overlying absorbing aerosols was estimated to be $9.2 \pm 6.6\mathrm{Wm}^{-2}$ and $-5.9 \pm 3.5\mathrm{Wm}^{-2}$, respectively; accounting for the frequency of occurrence of absorbing aerosols overlying overcast scenes, the all-sky direct and semidirect effect was estimated to be $1.0 \pm 0.7\mathrm{Wm}^{-2}$ and $-0.7 \pm 0.4\mathrm{Wm}^{-2}$, respectively. These radiative effect values, based on diurnal mean solar insolation, were presented as semi-empirical diurnal estimates, since by using cloud properties only at the time of satellite observation, they do not account for the variability of cloud albedo as a function of solar zenith angle during daytime.

[5] Most recently, *de Graaf et al*. [2012] inferred the above-cloud time-of-observation DARE of overcast scenes with overlying absorbing aerosols by comparing simulated aerosol-free cloud reflectance spectra (calculated from the UV to the shortwave infrared (SWIR)) with measured hyperspectral cloud reflectance from the Scanning Imaging Absorption Spectrometer for Atmospheric Chartography (SCIAMACHY). Averaging over August 2006, their estimated DARE over the southern Atlantic Ocean, off the coast of Africa, was $23 \pm 8\mathrm{Wm}^{-2}$. This technique is advantageous because it does not require a priori aerosol assumptions or retrievals, though the large footprint of SCIAMACHY (roughly $60 \times 30\,\mathrm{km}^2$) limits spatial sampling.

[6] The smoke aerosol spectral absorption can also be problematic for remote sensing retrievals of the underlying cloud optical properties, particularly for passive remote sensors such as MODIS, which rely primarily on reflectance measurements in visible (VIS) and near-infrared (NIR) spectral channels for retrieving cloud optical thickness. Absorption and scattering by overlying aerosols can introduce biases in the measured VIS/NIR cloud reflectance, which may then propagate into cloud optical property retrievals and, ultimately, into estimates of cloud and above-cloud aerosol radiative effect. *Haywood et al*. [2004] investigated potential smoke layer impacts on both MODIS and Advanced Very High Resolution Radiometer (AVHRR) retrievals of cloud optical thickness and effective particle radius with aircraft measurements of smoke properties obtained during the Southern African Regional Science Initiative (SAFARI 2000). Using the in situ measured smoke properties to simulate bi-spectral cloud retrieval look-up tables (LUTs) [*Nakajima and King*, 1990] both with and without an overlying smoke layer, they found that retrieved cloud optical thickness is expected to be low biased compared to the actual cloud optical thickness for both AVHRR and MODIS; retrieved effective particle radius is expected to be high biased for AVHRR retrievals using the 0.63 and 3.7 μm channel combination, but low biased for MODIS retrievals using the 0.86 and 1.63 μm channel combination. The bias in effective radius was due to the coupling of the VIS/NIR bias into the size retrieval for clouds with an optical thickness less than the asymptotic SWIR/MWIR (mid-wave infrared) reflectance value, and not due to the direct impact of absorbing aerosols in the SWIR/MWIR channels. A case study analysis of MODIS data concurrent with SAFARI 2000 confirmed the 0.86/1.63 μm low biases exhibited by the LUT simulations.

[7] *Wilcox et al*. [2009] also estimated potential biases in MODIS cloud optical thickness and effective particle radius retrievals. Specifically, MODIS retrievals of liquid water path (LWP), which depend on retrievals of both cloud optical thickness and effective particle radius, were compared with AMSR-E LWP retrievals, using the OMI UVAI to determine the presence of overlying smoke. Unlike the MODIS LWP retrievals, the AMSR-E LWPs are derived from microwave measurements, which are unaffected by aerosols. Wilcox et al. found minimal bias in effective radius retrievals and a low bias in optical thickness retrievals when the coincident OMI UVAI exceeded 2, suggesting that the underestimation was indeed caused by the overlying smoke layer.

[8] Active sensors have clear advantages over passive sensors in multilayer situations such as aerosols overlying clouds. CALIOP [*Winker et al*., 2009] can detect and identify multiple cloud and aerosol features within a single profile [*Liu et al*., 2004; 2009; *Hu et al*., 2009; *Omar et al*., 2009], including very optically thin layers, and can retrieve feature altitudes [*Vaughan et al*., 2009] and optical properties [*Young and Vaughan*, 2009]. The operational level-2 5 km aerosol and cloud layer products provide retrievals of aerosol and cloud optical thickness, as well as layer top and base altitudes. In addition to the standard CALIOP products, alternate optical property retrievals have been developed using CALIOP observations. For instance, using the depolarization ratio at 532 nm, the optical thickness of a thin layer (e.g., aerosols) can be retrieved when overlying an opaque cloud [*Hu et al*., 2007]. In a related technique, the ratio of measured backscatter at 532 and 1064 nm, the so-called color ratio, can be used to infer the optical thickness of absorbing aerosols overlying liquid

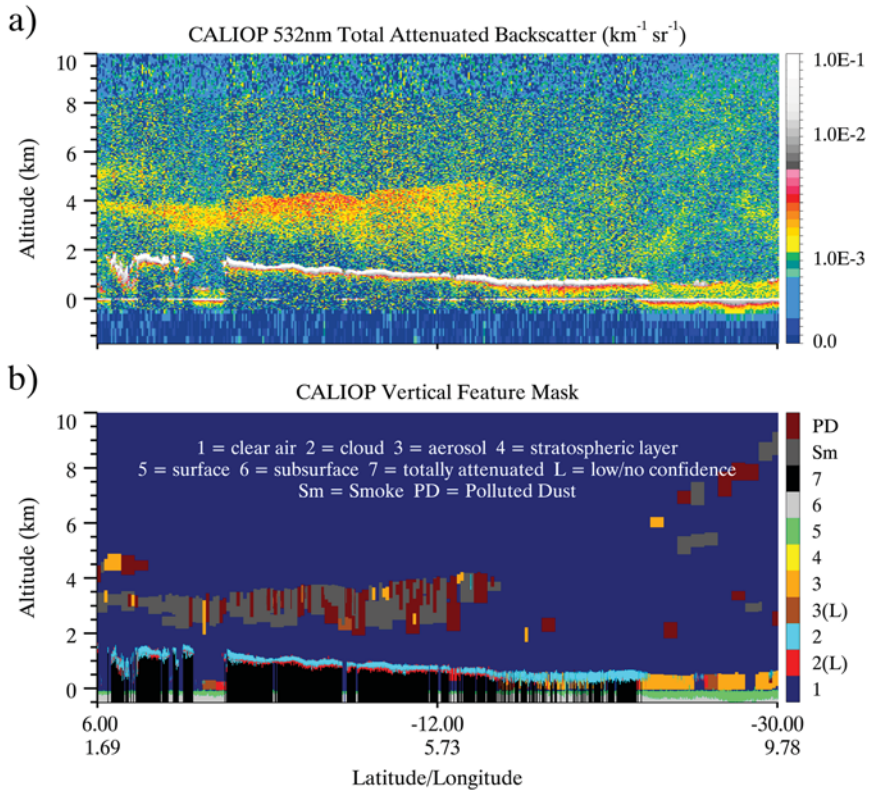

Figure 1. (a) CALIOP 532 nm total attenuated backscatter and (b) vertical feature mask feature classification obtained at 13:11:09Z (daytime orbit) on 26 August 2010.

clouds, provided the spectral dependence of the aerosol layer is well constrained [*Chand et al*., 2008].

[9] In the present study, Aqua MODIS optical property retrievals of the MBL clouds over the southeast Atlantic Ocean (off the coast of Namibia and Angola) are adjusted for biases resulting from attenuation by overlying absorbing smoke aerosols. The CALIOP 5 km aerosol layer product, collocated with the MODIS 1 km cloud products, is used for above-cloud absorbing aerosol detection and aerosol optical depth (AOD). Bias-adjusted cloud optical property retrievals are provided by a research-level version of the MODIS cloud optical property retrieval algorithm (MOD06) [*King et al*., 1998; *Platnick et al*., 2003] using liquid cloud forward LUTs modified to include above-cloud absorbing aerosol layers. Finally, the above-cloud time-of-observation direct aerosol radiative effect for overcast scenes is estimated using the CALIOP AOD and bias-adjusted MODIS cloud optical properties, and its sensitivity to the underlying cloud optical property biases is investigated. While this study addresses similar issues as in previous studies, it improves on the methodology by applying a fully coupled aerosol-cloud radiative transfer code at the pixel-level.

2. Data

2.1. CALIOP Layer Products

[10] We take advantage of the capability of CALIOP to detect optically thin and/or multiple layers to determine key properties of the absorbing aerosol layer over the southeast Atlantic Ocean. Specifically, the Version 3.01 CALIOP level-2 5 km aerosol layer product is used to define the aerosol layer top and bottom altitudes [*Vaughan et al*., 2009], as well as to provide estimates of the aerosol optical depth (AOD) derived from the 532 nm attenuated backscatter [*Young and Vaughan*, 2009]. Various data quality metrics and flags are used, following the best practice advice of the CALIPSO science team, to screen for reliable retrievals. These include the extinction Quality Control (QC), Cloud-Aerosol Determination (CAD) score, optical thickness uncertainty, and the horizontal averaging scale required for feature detection.

[11] The optically thin layer detection capability of CALIOP for a daytime orbit is illustrated in Figure 1, which shows along-orbit profiles of 532 nm total attenuated backscatter (Figure 1a) and feature classification type (and subtype for select aerosols) (Figure 1b), obtained from the Vertical Feature Mask, for a scene off the west coast of Africa on 26 August 2010 (13:11:09Z orbit). The backscatter plot (Figure 1a) shows a probable multilayer situation, with a broad region of modestly enhanced backscatter, located roughly between 6°N and 15°S latitude and 2 to 4.5 km altitude, overlying a very bright, geometrically thin layer at around 1 km altitude. CALIOP identifies the low-altitude, bright layer as clouds (light blue or red for type classification results with low/no confidence), while the broad overlying region is identified as aerosols, primarily of the smoke subtype (dark gray).

[12] It is interesting to note, however, that portions of the smoke layer in Figure 1b are identified as polluted dust (maroon) or other aerosol subtypes (orange or dark brown for low/no confidence). This apparent type misclassification can adversely affect smoke aerosol sampling. Other sampling issues

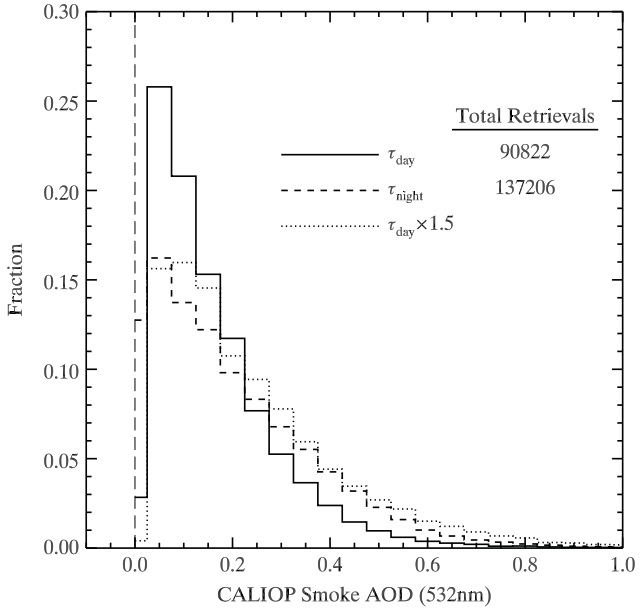

Figure 2. Histograms and total retrieval counts of CALIOP 532 nm smoke optical depths for daytime (solid line) and nighttime (dashed line) orbits over the southern Atlantic Ocean (30°S to 6°N, 20°W to 30°E during August and September 2006–2011. The dotted line shows the daytime histogram following multiplication of the AODs by 1.5.

are potentially also present in the daytime CALIOP data products. For instance, Figure 2 shows the probability distribution function (PDF) of CALIOP-derived daytime (solid line) and nighttime (dashed line) AOD, for smoke aerosol subtype only, obtained from 6 years (2006–2011) of August and September observations over the southeast Atlantic Ocean (ocean-only retrievals in the region bounded by 6°N to 30°S latitude and 20°W to 20°E longitude). Retrieval counts are shown in the upper right corner of the plot. Note that the daytime retrieval count is roughly 34% smaller than the nighttime count (90,822 total daytime retrievals and 137,206 total nighttime retrievals). Furthermore, the daytime PDF is appreciably different from the nighttime PDF and is weighted toward smaller AOD.

[13] Such sampling issues are likely caused by a smaller signal-to-noise ratio (SNR) during daytime as a result of solar background illumination. CALIOP detection thresholds are necessarily higher during daytime, which are expected to decrease sensitivity to optically thin layers within a given lidar profile and reduce aerosol detection capability [*Winker et al*., 2012]. Thus, not only are optically thin aerosol layers less likely to be detected and be assigned optical property retrievals during daytime, i.e., the horizontal sampling is decreased (as shown by the retrieval counts in Figure 2), but the full extent of the geometrical thickness of the aerosol layers is also less likely to be captured (decrease in vertical sampling; see, e.g., Figure 5), resulting in low-biased AOD. Both phenomena likely contribute to the smaller daytime AOD retrievals compared to nighttime illustrated by the PDFs in Figure 2. Low SNR issues are also likely exacerbated for smoke aerosols, which, due to being composed of absorptive black carbon, have a larger lidar ratio (i.e., extinction to backscatter ratio) than other aerosol types, and thus less signal at 532 nm for a fixed AOD (Vaughan, personal communication, 2012). Further sampling issues also exist due to layer misidentification, again a potential result of the lower daytime SNR, as becomes evident by the polluted dust (and other aerosol subtype) features within the predominantly smoke-identified aerosol layer of Figure 1.

[14] Returning to Figure 2, note that scaling the daytime AOD retrievals, here by a factor of 1.5, causes the daytime PDF (dotted line) to align better with the nighttime PDF, though there appears to be an overestimation of the fraction of larger AOD. This is somewhat misleading, however, as this scaling cannot account for horizontal sampling issues (i.e., undetected optically thin aerosol layers) which, if the AOD retrieval itself is unbiased, can be expected to skew the PDF (as well as the mean and median retrieved AOD) toward larger values. Additionally, this scaling implicitly assumes that there is not a significant diurnal variation in the above-cloud aerosols over the southeast Atlantic Ocean. Note that over portions of the continent itself, a diurnal cycle in the AOD has been observed at some AERONET sites [e.g., *Eck et al*., 2003], possibly due to a diurnal burning cycle. A subsequent modeling study (using a three-dimensional aerosol microphysical, transport, and radiation model) was able to reproduce regional aerosol optical properties comparable to available observations, but was unable to reproduce the diurnal cycle of AOD, suggesting that the AERONET sites are sensitive to very local sources which are quickly dispersed [*Matichuk et al*., 2006]. This implies that diurnal variations caused by a diurnal burning cycle are unlikely to survive for those aerosols transported long distances over the southeast Atlantic. Furthermore, the underlying assumption of little diurnal variation in the aerosol properties is consistent with previous investigations in this region [e.g., *Chand et al*., 2009]. While caution is warranted when applying a single-factor scaling, it nevertheless provides a reasonable approach to account for low-biased daytime AODs and to estimate the sensitivities of both the cloud property retrieval bias adjustments and the resulting direct aerosol radiative effect to uncertainties in above-cloud AOD.

[15] An alternate method to address the daytime sampling, on the other hand, is to include other aerosol subtypes, in particular polluted dust. The CALIOP polluted dust subtype was developed for cases of dust mixing with biomass burning smoke and was derived from a mixture of the desert dust and biomass burning aerosol types identified by AERONET cluster analysis [*Omar et al*., 2005, 2009]. Though its size distribution is more weighted toward the coarse mode than smoke, and it is somewhat less absorbing (the imaginary refraction indices at 532 nm are 0.0234*i* and 0.0109*i* for smoke and polluted dust, respectively), a significant difference in AOD between the two aerosol types is not expected. In this study, results will be presented from exploring all these possibilities, i.e., using both raw CALIOP AOD and scaled AOD, as well as the raw and scaled combined smoke/polluted dust AOD.

2.2. MODIS Cloud Optical Property Products

[16] The MODIS cloud optical property retrievals [*King et al*., 1998; *Platnick et al*., 2003], based on the bi-spectral look-up table (LUT) technique developed by *Nakajima*

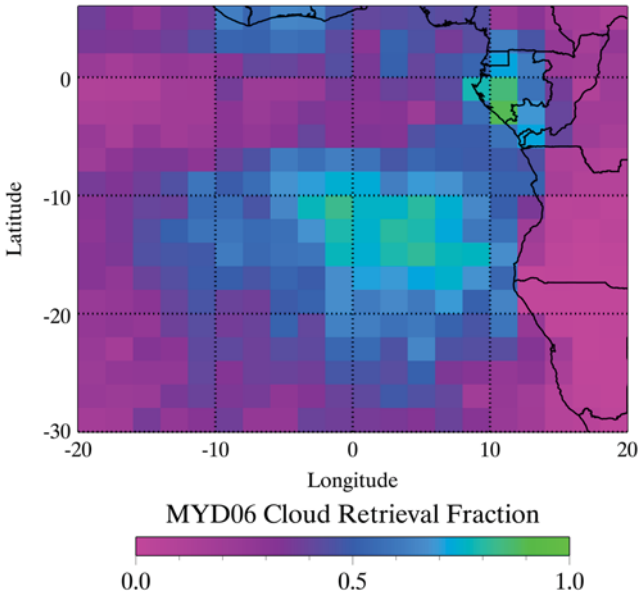

Figure 3. MYD06 Collection 6 liquid cloud retrieval fraction (i.e., fraction of pixels with successful COT and r_e retrievals) for pixels collocated with the CALIPSO ground track during August and September 2006–2011 aggregated to a 2° grid.

and King [1990] and *Platnick and Twomey*, [1994], provide estimates of both cloud optical thickness (COT) and effective particle radius (r_e) for the liquid and ice cloud phases. While the archived data product name for these retrievals is MOD06 and MYD06 for Terra and Aqua, respectively, we will generically refer to the retrieval algorithm as MOD06 because the same algorithm is used for both sensors. The standard MOD06 retrieval mainly pairs one of three nonabsorbing (or relatively nonabsorbing) VIS/NIR channels (0.66, 0.86, and 1.24 μm), sensitive mainly to COT, with an absorbing SWIR or MWIR channel that is sensitive to r_e. The specific VIS/NIR channel selection depends on the underlying surface type (i.e., 0.66 μm over land, 0.86 μm over water, and 1.24 μm over snow/ice). For the standard MOD06 retrieval used in this study, 2.1 μm is the SWIR channel of choice for effective particle radius retrievals ($r_{e2.1}$); because the focus is on the southeast Atlantic Ocean, all COT retrievals used here are derived from the 0.86 μm NIR channel only.

[17] In the present investigation, all MODIS cloud retrievals are performed using a research-level version of MOD06 that incorporates most of the significant changes and advancements that constitute the upcoming (at the time of writing) Collection 6 reprocessing effort. These include using full LUTs across the full range of COT rather than asymptotic theory at large COTs, enhancements in the DISORT [*Stamnes et al*., 1988] forward radiative transfer (RT) code used for LUT generation, and various modifications to ancillary data use. Perhaps the most significant change, however, and the one most pertinent to the present investigation, is the handling of ocean surface reflectance. In the current Collection 5 MOD06, the ocean surface is assumed to be a Lambertian reflector with a diffuse illumination (below cloud) albedo of 5%, typically suitable underneath clouds with optical thickness greater than about 3. For Collection 6, a Cox-Munk BRDF [*Cox and Munk*, 1954a, 1954b] is introduced to more accurately account for the angular and wind speed dependence of ocean surface reflectance, which manifests itself most notably at Sun glint geometries. This new ocean surface model is expected to especially impact retrievals of optically thin clouds (COT roughly 3 or less), when the ocean surface receives more direct illumination. It should be pointed out that, even though this investigation uses the Collection 6 MOD06 algorithms, the current publically available Collection 5 retrievals (the operational version at the time of writing) will suffer the same effects from above-cloud absorbing aerosols as those shown here.

[18] Similar to CALIOP, the MODIS products are also susceptible to sampling issues. Because MOD06 relies on the assumption of homogeneous plane-parallel clouds, the retrievals may not be useful at cloud edges or for other partly cloudy scenes where cloud inhomogeneity and 3-D effects can be significant. Such pixels can be identified by subpixel tests (using the 250 m 0.66 and 0.86 μm VIS channels) or cloud edge detection tests (defined by the MODIS cloud mask, MOD35) [*Zhang and Platnick*, 2011; *Pincus et al*., 2012], and in Collection 5 are not processed. Retrievals are attempted on this partly cloudy pixel population in the Collection 6 code, though in many cases the retrieval fails (observations are outside the solution space) and the solution nearest to the LUT space is provided. Both partly cloudy and failed retrieval pixels are excluded from the present study; together they account for roughly 27% of the pixels identified by MOD35 as being not clear over this region and season.

[19] The collocation of MODIS and CALIOP is accomplished using the method detailed in *Holz et al*. [2008]. Spatial sampling is confined to the CALIPSO ground track and is further constrained by the aforementioned sampling limitations of both CALIOP and MODIS. Moreover, the collocation itself can introduce further uncertainties: Collocation at ground level can result in a large parallax effect, particularly for large viewing zenith angles (VZA) or clouds at high altitudes (or, worse, when both occur simultaneously). The parallax effect is not expected to be significant here, however, as the MODIS VZA for collocated pixels is relatively small (the CALIPSO ground track is only roughly 200 km off MODIS nadir) and the MBL cloud top altitudes are typically less than 2 km (see Figure 5 below).

[20] Figure 3 shows a 2° aggregation of the MYD06 Collection 6 liquid phase cloud optical property retrieval fraction for pixels collocated with the CALIPSO ground track during August and September 2006–2011. Here cloud retrieval fraction is defined as the number of collocated MODIS pixels with successful liquid cloud COT and r_e retrievals divided by the total number of collocated MODIS pixels within each grid box. Over the southeast Atlantic, the cloud retrieval fraction can be quite large, approaching roughly 0.8 off the coast of Namibia. It is important to note that the cloud retrieval fraction is smaller than the cloud fraction derived from the cloud mask product (MYD35), since not all pixels identified by MYD35 as cloudy have successful COT and r_e retrievals (largely a result of the cloud edge issues discussed above). Nevertheless, the spatial pattern shown in Figure 3 is in good agreement with the Aqua MODIS level-3 (MYD08_M3) global gridded monthly mean cloud fractions for August and September (not shown).

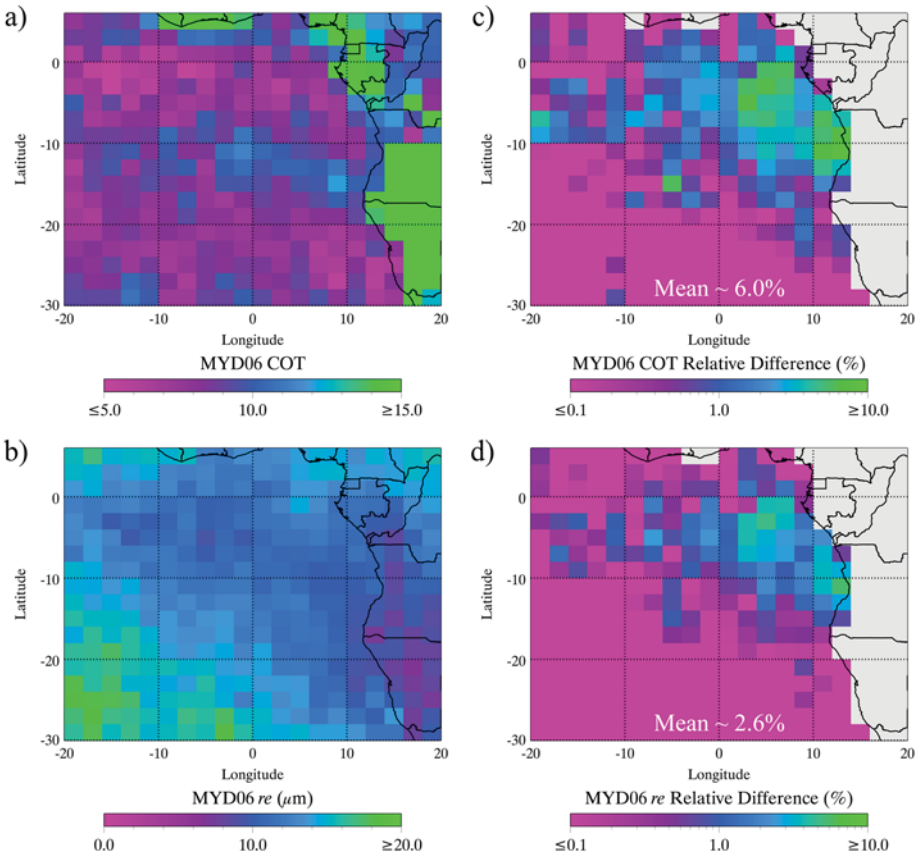

Figure 4. MYD06 Collection 6 liquid cloud mean retrieved (a) COT and (b) r_e for pixels collocated with the CALIPSO ground track during August and September 2006–2011 aggregated to a 2° grid. Retrieval differences after adjusting for above-cloud aerosol absorption, averaged over all collocated ocean-only cloudy pixels, are shown for (c) COT and (d) r_e. Because the retrieval adjustment is only performed over the ocean, grid boxes in which the surface is predominantly land are shaded gray in Figures 4c and 4d.

[21] The 2° aggregation of MYD06 mean retrieved COT and r_e without accounting for overlying aerosols are shown in Figures 4a and 4b, respectively. The time period and geographical region are the same as for Figure 3 and subsequent figures. COT is relatively uniform off the coast, whereas r_e generally increases toward the southwest.

3. CALIOP Aerosol Layer Statistics

[22] Six years of the CALIOP Version 3.01 5 km Cloud and Aerosol Layer Products (2006–2011) for August and September have been used to generate statistics of the spatial distribution of the properties of absorbing aerosol and underlying clouds over the southeast Atlantic Ocean. Here CALIOP observations are restricted to the geographic region bounded by 6°N to 30°S and 20°W to 20°E. The aerosol statistics consist of mean layer top and bottom altitudes, as well as 532 nm layer AOD; cloud statistics include only cloud top altitude (CALIOP MBL cloud base altitudes can be significantly biased high as the signal is quite often totally attenuated within the cloud, as is evident in Figure 1). Only daytime CALIPSO orbits are considered here due to the daytime-only constraint on the MYD06 cloud optical property retrievals. The CALIOP Feature Classification Flags, included in both the Aerosol and Cloud Layer Products, are used to filter for aerosol and cloud type; here only the smoke type is considered for the absorbing aerosol layer, while for clouds four subtypes are considered, namely, transparent and opaque low overcast, transition stratocumulus, and low broken cumulus. Additionally, the aerosol layer products are further screened for data quality using the 532 nm layer optical depth uncertainty (must be less than 99.9), the 532 nm extinction QC flag (must be less than 2), and the CAD score (must be less than −30); because only cloud top altitude is considered, only the CAD score is used (greater than 30), with no additional optical property quality screening.

[23] Figure 5 shows the daytime (Figure 5a) and nighttime (Figure 5b) meridional mean smoke and cloud layer top (solid and dashed lines, respectively) and smoke bottom (dotted line) altitudes, as well as low/stratus cloud fraction (gray lines), averaged every 2° longitude for the latitude zone between 6°N and 30°S. Here the coast of Africa is located roughly around 10°E–15°E longitudes. The two mean layers either fully converge (nighttime) or nearly converge (daytime) to the east of this boundary over the continent, though the corresponding cloud fractions are quite low. Moving west of this boundary, however, over the southern Atlantic Ocean, despite the increase of mean cloud top altitude (by roughly 0.5 km) with increasing boundary layer height, the two layers are consistently separated by roughly 2 km during daytime and 1.5 km during nighttime. Statistically, this suggests that off the coast there is little entrainment of the

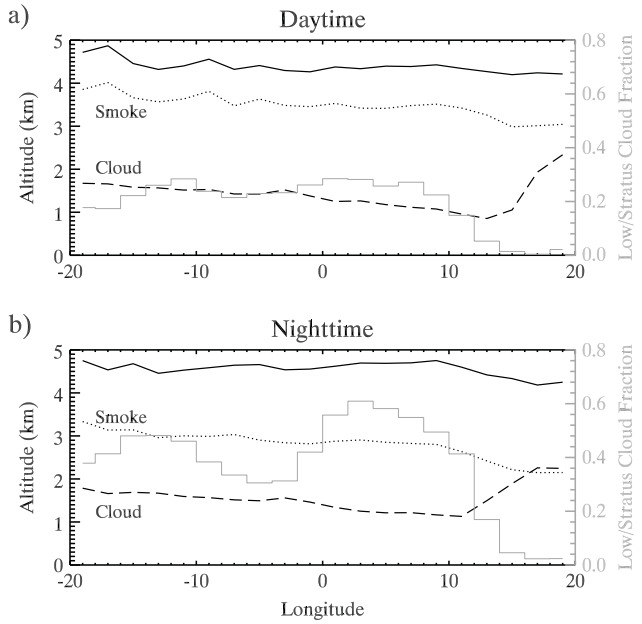

Figure 5. Meridionally averaged smoke aerosol subtype top and bottom heights (solid and dotted lines, respectively), and low/stratus cloud top height (dashed line) and cloud fraction (gray line), calculated from 6 years of August and September CALIOP (a) daytime and (b) nighttime observations (2006–2011). Data are located between 6°N and 30°S.

smoke layer into the underlying MBL cloud deck. This does not necessarily mean that entrainment never occurs, however, since the sensitivity of CALIOP to the optically very thin aerosol layer base may be affecting detection. Note also that the potential daytime vertical sampling issues discussed earlier in section 2.1 are evident here, as the detected smoke base altitude is over 0.5 km higher during the daytime than during the nighttime.

[24] Gridded layer statistics, calculated on a 2° grid, are shown in Figure 6. Here grid boxes with layer detection frequencies smaller than 20% of the mean count of detected aerosol layers for the entire region are excluded. This additional screening removes statistically insignificant grid boxes, particularly in the southwest portion of the region, where CALIOP infrequently observes, or is unable to detect, smoke-type aerosols. Shown here are the CALIOP mean smoke base altitude (Figure 6a), mean cloud top altitude (Figure 6b), mean layer separation (i.e., smoke base altitude minus cloud top altitude) (Figure 6c), and mean smoke layer AOD at 532 nm (Figure 6d). Gray regions denote missing data, primarily due to grid boxes with insufficient aerosol layer counts. Cloud top altitude exhibits minima (less than 1 km) over the ocean near the coast, and increases moving westward, to between 1.5 and 2 km near 20°W longitude (consistent with Figure 5, where the minimum is located near 11°E). Smoke base altitude generally increases moving toward the southwest, from roughly 3 km to 4 km or higher. A trend in mean layer separation (Figure 6c) is discernible, with separation distance decreasing from south to north (from, respectively, approximately 3 km to 2 km or smaller). Note also the negative layer separation (i.e., layer overlap) over the continent, due to the location of biomass burning. There is little evidence of entrainment during the daytime over the Atlantic, however, as the fraction of profiles in this region with smoke base altitude less than cloud top altitude (not shown here) is near zero, though again the reduced sensitivity of CALIOP to optically thin scattering layers during daytime may be a contributing factor. Interestingly, an analysis of nighttime orbits (also not shown) does in fact indicate potential aerosol entrainment into the cloud over the Atlantic, particularly in the northwest section of the region where the detected smoke base is below the cloud top in up to 10% of the profiles in some grid boxes.

[25] As expected, the mean smoke layer AOD in Figure 6b is greatest over the continent (near 0.5) close to the biomass burning source. Moving westward over the southeastern Atlantic, in the general direction of atmospheric transport, the mean smoke layer AOD gradually decreases to less than 0.25. Analysis of the less noisy nighttime orbits (again not shown here) reveals a much more extensive smoke layer, as well as larger mean AOD, suggesting again that the daytime AOD is indeed systematically underestimated (as previously mentioned in Figure 2 discussion).

4. Correcting MOD06 for Absorbing Aerosol Extinction

[26] To account for the effects of overlying absorbing aerosols on MOD06 cloud optical property retrievals, combined cloud-aerosol optical property LUTs have been created. This is accomplished by inserting an absorbing aerosol layer of varying optical thickness over the liquid phase cloud layer in the forward RT calculations. Similar to the standard MOD06 LUTs, particularly for the upcoming Collection 6, the new tables are created under the assumption of an otherwise transparent atmosphere (gaseous absorption is added during the retrieval process along with a Rayleigh correction for the VIS channel), with Cox-Munk ocean surface reflectance averaged over all wind directions at three wind speeds (3, 7, and 15 m s^{-1}). The LUTs are otherwise identical to their MOD06 counterparts with respect to COT, r_e, and angle space, with the exception of the VZA, which is constrained to the angle space typical of the collocated pixels along the CALIPSO track.

[27] The above-cloud aerosol bulk optical and microphysical properties are estimated based on the absorbing aerosol models developed for the MODIS Collection 5 Aerosol Product (MOD04). The MOD04 aerosol models define aerosol size distributions and refractive indices dependent solely on prescribed AOD at 0.55 μm (MODIS band 4; note that the absorbing aerosol model used here assumes a single index of refraction, 1.51–0.02*i*, at all wavelengths). Band-averaged scattering properties (scattering phase function, single-scatter albedo, asymmetry parameter, etc.) for the relevant MODIS spectral channels (0.86, 2.1 μm) are computed using the MIEV Mie code [*Wiscombe*, 1980] for distinct wavelengths and subsequent integration over the detector mean spectral response functions. The resulting bulk optical properties are generally in good agreement with those of *Levy et al*. [2009] even though the operational MOD04 bulk properties are calculated at the band-center wavelength, and not averaged over the MODIS spectral response functions. The bulk asymmetry parameter (g), single scatter albedo (ω_o), and extinction efficiency (Q_e) calculated for an aerosol layer with AOD 0.5 at wavelength 0.55 μm are shown in Figure 7.

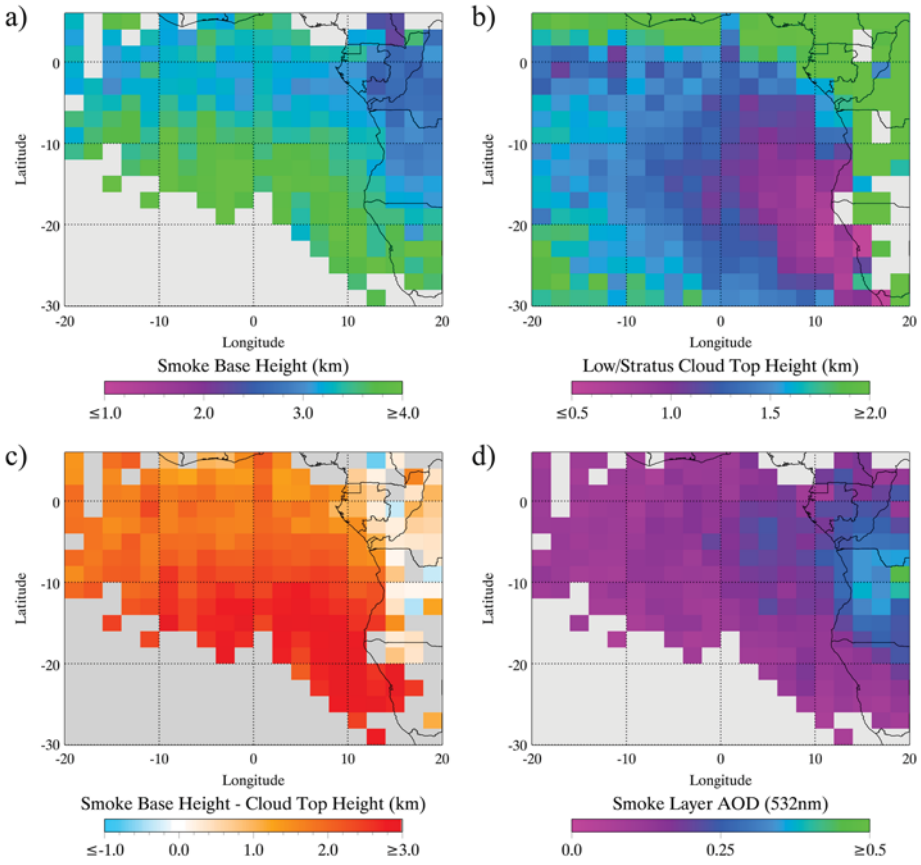

Figure 6. August/September (2006–2011) mean daytime CALIOP (a) smoke layer base altitude, (b) cloud layer top altitude, (c) smoke/cloud layer separation (i.e., smoke layer base altitude minus cloud layer top altitude), and (d) smoke layer AOD at 532 nm.

[28] Using the aerosol bulk properties, five modified liquid phase cloud LUTs are created, one each for five different above-cloud AODs (0.05, 0.1, 0.2, 0.4, and 0.8 at 0.55 µm). For LUT selection, the five AODs are scaled to the CALIOP wavelength of 0.532 µm using the MOD04 wavelength-dependent bulk extinction efficiencies (Q_e). Figure 8 shows an example of a standard MOD06 water cloud LUT (black lines) and the corresponding coupled aerosol-cloud LUT (red lines). Here the above-cloud AOD is 0.4 at wavelength 0.55 µm (a somewhat extreme value given the AOD distribution in Figure 2), and the surface wind speed is 3 m s^{-1}. Similar to the findings of *Haywood et al*. [2004], accounting for above-cloud aerosol absorption shifts the LUT toward smaller VIS reflectances, yielding larger COT retrievals for a constant value of VIS reflectance.

[29] A given cloudy MODIS pixel is deemed to have above-cloud absorbing aerosols if the collocated CALIOP Aerosol Layer Product provides an AOD retrieval of sufficient quality within the pixel's field of view. Specifically, the 532 nm feature optical depth uncertainty must be less than 99, the extinction QC flag less than 2, the CAD score less than −30, and layer top pressure smaller than the MYD06 cloud top pressure; an additional constraint is provided by the CALIOP feature subtype (e.g., smoke,

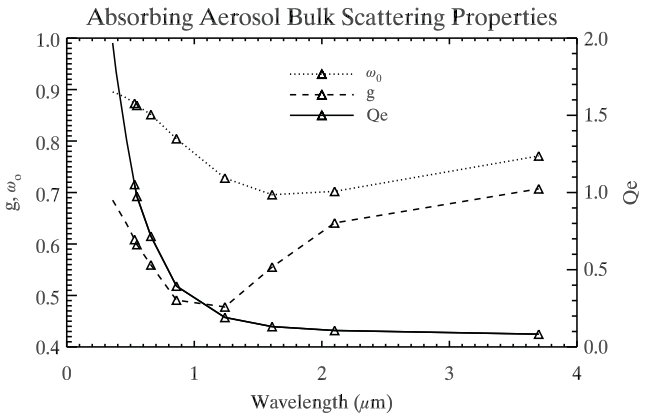

Figure 7. Aerosol bulk scattering properties derived from the MODIS Collection 5 Aerosol Product (MOD04) absorbing aerosol model. Shown here are the asymmetry parameter (g), single-scatter albedo (ω_o), and extinction efficiency (Q_e) as a function of wavelength, assuming an AOD of 0.5 at wavelength 0.55 µm. Triangles denote the spectral locations of the MODIS cloud property retrieval channels, as well as the 0.55 µm MODIS aerosol channel and the 0.532 µm CALIOP wavelength.

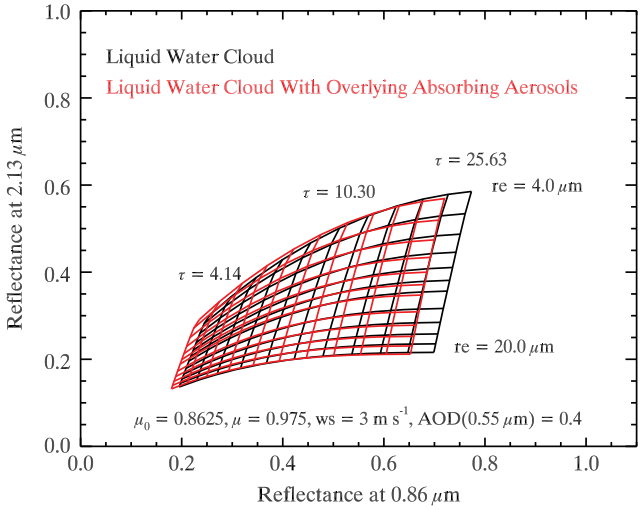

Figure 8. Visual representation of bi-spectral cloud optical property retrieval look-up tables (LUT). The standard MOD06 liquid water cloud LUT is shown in black; the new coupled cloud-aerosol LUT is shown in red. Attenuation at 0.86 μm by the above-cloud absorbing aerosols shifts the LUT toward smaller 0.86 μm reflectances, yielding larger COT retrievals for the same reflectance.

polluted dust). Aerosol-contaminated cloudy pixels then follow an alternate retrieval path within the experimental MOD06, in which the CALIOP 532 nm AOD is used to identify an appropriate aerosol/cloud LUT (i.e., a linearly interpolated LUT from the nearest two of the five defined above-cloud AODs). From here the MOD06 retrieval proceeds as usual, providing a bias-adjusted cloud optical property retrieval accounting for above-cloud absorbing aerosol attenuation.

[30] The gridded mean relative increases in MYD06 COT and r_e retrievals after adjusting for the attenuation by above-cloud absorbing aerosols are shown in Figures 4c and 4d, respectively. Here retrieval differences are averaged over all cloudy liquid water phase MODIS pixels (excluding partial retrievals and cloud edge pixels which are expected to be partly cloudy to some extent [*Pincus et al.*, 2012]) during the entire 6 year period (August/September 2006–2011). Bias-adjusted MOD06 retrievals are performed for ocean-only pixels in which CALIOP detects above-cloud smoke type aerosols. Grid boxes over predominantly land surfaces are shaded gray, though some grid boxes containing the coast are nevertheless retained as the ocean-only retrieval count in each is sufficiently large. As expected, the COT retrieval differences are greatest near the coast, where the above-cloud AOD is generally larger (see Figure 6d), and gradually decrease westward. Averaged over the entire region, the retrieved COT increases by roughly 6%. Note that while generally smaller than the COT differences, r_e also exhibits noticeable differences, with a regional mean increase of roughly 2.6%. An analysis of the retrievals (not shown here) reveals that these r_e differences are a strong function of COT and are much less dependent on the overlying AOD (one can see in Figure 7 that the aerosol extinction and single scattering albedo are significantly weaker at 2.1 μm than at 0.86 μm). The r_e differences in fact increase rather dramatically with decreasing COT. They can therefore be attributed to LUT non-orthogonality (i.e., the COT and r_e retrievals are not completely independent), particularly at small COT.

[31] Figure 9 shows the histograms of MYD06 liquid cloud optical thickness for the entire 6 year period for pixels with and without an overlying absorbing aerosol layer (dashed and solid black lines, respectively), as determined using the CALIOP smoke-only subtype (Figure 9a) and smoke and polluted dust subtypes (Figure 9b). Also shown are the histograms of the bias-adjusted MYD06 COT using the unscaled and scaled CALIOP above-cloud AOD (blue and red lines, respectively). Note that the polluted cloudy pixels retrieved without the aerosol correction generally exhibit smaller COT than do the clean cloudy pixels, as expected due to the above-cloud attenuation of the VIS channel. In addition, the increased horizontal sampling due to inclusion of the polluted dust aerosol subtype is evident when comparing the polluted cloudy pixel counts in Figures 9a and 9b. Adjusting COT for the effects of above-cloud absorbing aerosols shifts the histogram toward

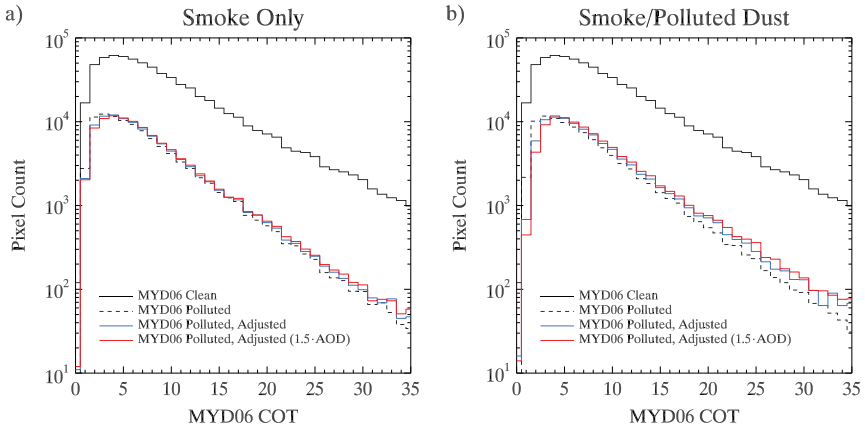

Figure 9. Histograms of MYD06 unadjusted cloud optical thickness for cloudy pixels with and without CALIOP above-cloud absorbing aerosols (dashed and solid black lines, respectively), as well as bias-adjusted cloud optical thickness using the CALIOP un-scaled and scaled (x1.5) above-cloud AOD (blue and red lines, respectively). (a) Retrievals using CALIOP smoke-only subtype AOD. (b) Retrievals using CALIOP smoke and polluted dust subtype AOD.

Table 1. Scalar Statistics of MYD06 Cloud Optical Properties

CALIOP Aerosol Type		Cloud Optical Thickness			Cloud Effective Radius		
		Mean	Median	σ	Mean	Median	σ
Smoke only	Clean	8.9	7.0	7.1	12.9	11.8	5.3
	Polluted, uncorrected	6.5	5.2	4.7	10.9	9.9	4.3
	Polluted, corrected	7.7	6.0	8.8	12.1	10.9	4.9
	Polluted, corrected with AOD scale	8.9	6.4	14.1	12.8	11.4	5.4
Smoke and polluted dust	Clean	9.1	7.1	7.2	13.0	11.9	5.3
	Polluted, uncorrected	7.1	5.7	5.1	11.0	10.0	4.3
	Polluted, corrected	7.9	6.3	6.5	11.9	10.8	4.8
	Polluted, corrected with AOD scale	8.7	6.7	9.9	12.5	11.2	5.2

larger values, as expected. Moreover, scaling the above-cloud AOD to account for the observed differences in the daytime/nighttime CALIOP data further shifts the retrieved COT toward larger values.

[32] Table 1 provides the mean, median, and standard deviation of MYD06 ocean-only COT and r_e for both the smoke-only and smoke/polluted dust aerosol subtypes. The clean cloudy pixel retrievals have larger mean and median COT and r_e than the retrievals under polluted conditions, but with aerosol ignored (note that adding the polluted dust subtype modifies the pixel sampling, and thus results in different clean cloudy pixel statistics). When the above-cloud aerosol attenuation is accounted for, larger mean and median adjusted COT and r_e are obtained for the polluted cloudy pixels. Note that the rows labeled "Corrected With AOD Scaling" refer to scaling CALIOP above-cloud AOD retrievals by the factor 1.5 as discussed in section 2.1 and Figure 2. Interestingly, despite the sampling differences between the different pixel populations, there is little statistical difference between the clean and bias-adjusted polluted cloudy pixels using the scaled AODs (both smoke-only and smoke/polluted dust). The good agreement in the statistics shown here may be partly fortuitous, however, as daytime CALIOP sampling issues cannot be entirely resolved, and thermodynamic or meteorological factors may also affect daytime/nighttime AOD differences.

5. Aerosol and Cloud Radiative Effect Analysis

[33] Estimating the above-cloud direct aerosol radiative effect (DARE) of the absorbing aerosols is accomplished through solar broadband radiative transfer (RT) calculations using the RRTMG-SW RT code [*Clough et al.*, 2005; *Iacono et al.*, 2008]. In RRTMG-SW, gaseous absorption is treated using the correlated *k* approach; the delta-Eddington [*Joseph et al.*, 1976] two-stream approximation [*Meador and Weaver*, 1980; *Oreopoulos and Barker*, 1999] is used for scattering. Broadband solar fluxes are calculated from 14 wideband fluxes of variable width between 0.2 and 12.0 μm. Here the top of atmosphere (TOA) DARE associated with a cloudy pixel is defined as

$$\mathrm{DARE}_{\mathrm{cloudy}} = F^{\uparrow}_{\mathrm{cloud}} - F^{\uparrow}_{\mathrm{cloud+aerosol}} \quad (1)$$

where $F^{\uparrow}_{\mathrm{cloud}}$ and $F^{\uparrow}_{\mathrm{cloud+aerosol}}$ are the upwelling broadband TOA SW fluxes for the cloud only and the cloud with overlying aerosol, respectively. Another measure of aerosol radiative effect, the TOA DARE per unit AOD, or radiative forcing efficiency (RFE), can be obtained by normalizing $\mathrm{DARE}_{\mathrm{cloudy}}$ by the above-cloud AOD, such that

$$\mathrm{RFE} = \mathrm{DARE}_{\mathrm{cloudy}}/\mathrm{AOD} \quad (2)$$

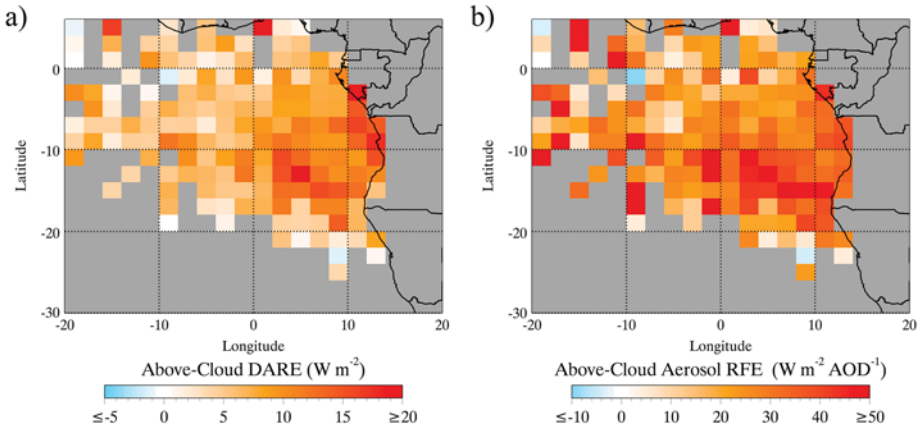

Figure 10. Gridded mean instantaneous (i.e., time of observation) above-cloud direct aerosol radiative effect (DARE) at (a) TOA and (b) aerosol radiative forcing efficiency (RFE), averaged over the 6 year CALIOP/MODIS collocated data record (August/September 2006–2011), for cloudy MODIS pixels for which CALIOP produces a reliable above-cloud smoke subtype aerosol retrieval.

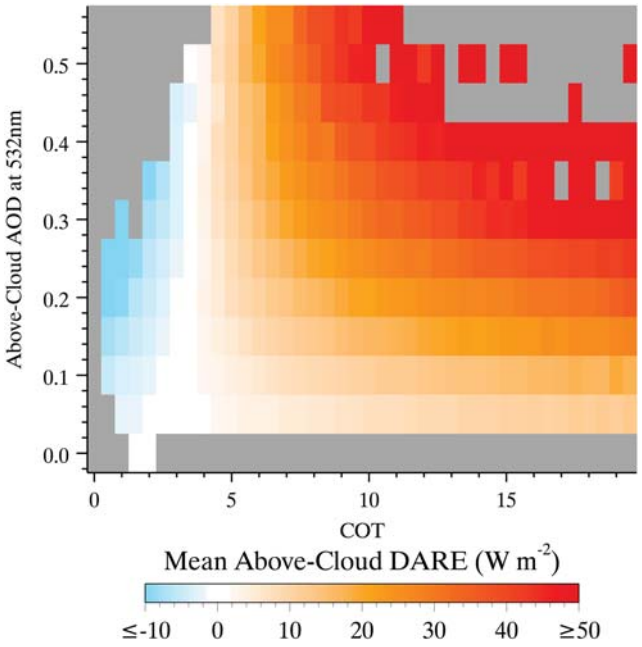

Figure 11. Mean instantaneous (i.e., at time of observation) above-cloud DARE at TOA (equation (1)), for cloudy MODIS pixels for which CALIOP produces reliable above-cloud smoke subtype aerosol retrievals, as a function of both COT and above-cloud AOD.

[34] RFE is useful because it removes in effect the DARE dependence on above-cloud AOD and isolates the impacts of the change in the underlying cloud properties.

[35] The broadband RT calculations depend on both COT and r_e, in addition to AOD in the case of cloud with overlying aerosol. It is evident from equation (1) that for absorbing aerosols overlying bright clouds $DARE_{cloudy}$ (hereafter referred to simply as DARE) is positive (i.e., warming) since $F^{\uparrow}_{cloud+aerosol}$ is smaller than $F^{\uparrow}_{cloud}$ due to the aerosol attenuation. Note that the calculations presented here pertain to the time of observation only (near local noon for Aqua overpass), i.e., they are instantaneous values. Because the biases in r_e are caused by biases in COT (as discussed in section 4), the differences in DARE discussed below are framed in terms of COT.

[36] All above-cloud absorbing aerosol properties are provided by CALIOP, including AOD and layer top and base altitudes. The MOD04 absorbing aerosol model is used to scale the spectrally dependent AOD to the 14 solar bands of RRTMG-SW, as well as to provide band-averaged scattering and absorption properties (i.e., single-scattering albedo and asymmetry parameter). Cloud properties are provided by Aqua MODIS, and include r_e, LWP (a function of both COT and r_e), and cloud top pressure (CTP). Atmospheric profile information is obtained from the ancillary data sets used in MOD06, namely, the National Centers for Environmental Prediction (NCEP) Global Data Assimilation System (GDAS) reanalysis product [*Derber et al.*, 1991]. Additionally, the instantaneous TOA downwelling solar flux (adjusted for Earth/Sun distance) is calculated from the total solar irradiance, pixel-level solar zenith angle (obtained from the MODIS Level 1 Geolocation product (MOD03)), and day of year.

[37] The gridded mean instantaneous TOA DARE (Wm^{-2}) and RFE ($Wm^{-2}AOD^{-1}$) for cloudy MODIS pixels in which CALIOP provides a reliable above-cloud smoke subtype aerosol retrieval are shown in Figures 10a and 10b, respectively. Data are averaged over the entire 6 year collocated CALIOP/MODIS dataset (August/September 2006–2011). Gray regions denote grid boxes with insufficient smoke subtype layer counts (i.e., less than 20% of the mean detected layer count for the entire region). Note that the DARE and RFE estimates shown here are calculated using the bias-adjusted cloud optical properties. It is evident that DARE is strongest near the coast, in roughly the same

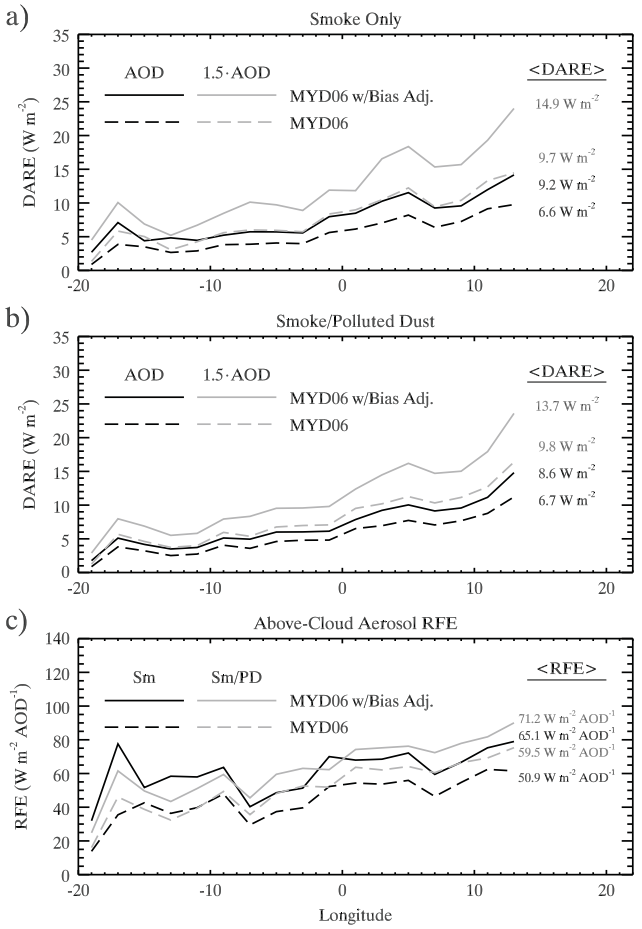

Figure 12. Meridional mean instantaneous above-cloud DARE at TOA, averaged over the 6 year CALIOP/MODIS collocated data record (August/September 2006–2011), for cloudy MODIS pixels for which CALIOP produces (a) reliable above-cloud smoke subtype and (b) smoke or polluted dust subtype aerosol retrievals (i.e., only the polluted cloudy pixels). The solid and dashed lines denote TOA DARE using the bias-adjusted and non-adjusted MYD06 COT, respectively; the black and gray lines denote the use of CALIOP-derived above-cloud AOD and scaled AOD (x1.5), respectively. Also shown is the (c) meridional mean RFE for smoke subtype aerosols (Sm) and combined smoke/polluted dust (Sm/PD). Mean values for each case, averaged over the entire domain (30°S to 6°N, 20°W to 30°E), are shown at the right of each plot.

Table 2. Scalar Statistics of Estimated TOA Direct Aerosol Radiative Effect

CALIOP Aerosol Type	MYD06 Bias Adjustment	DARE ($W\,m^{-2}$)		All Cloud DARE ($W\,m^{-2}$)		$<\Delta DARE>$($W\,m^{-2}$)	
		Mean	σ	*Mean*	σ	*Mean*	σ
Smoke only	No	6.6	9.8	0.3	2.6	16.8	12.6
	Yes	9.2	11.0	0.5	3.2	19.5	14.9
Smoke only, with AOD scale	No	9.7	13.9	0.5	3.7	24.7	18.0
	Yes	14.9	17.0	0.7	4.9	29.9	22.9
Smoke and polluted dust	No	6.7	9.2	0.8	3.9	15.3	12.0
	Yes	8.6	10.1	1.1	4.6	17.2	13.7
Smoke and polluted dust, with AOD scale	No	9.8	13.1	1.2	5.6	22.6	17.1
	Yes	13.7	15.7	1.7	7.1	26.5	21.1

region where the mean above-cloud AOD peaks, with mean instantaneous values near $20Wm^{-2}$.

[38] Note also in Figure 10 that mean DARE is near zero or negative in some grid boxes. It was pointed out by *Twomey* [1977b] that an aerosol layer can result in a net warming (TOA DARE > 0) or cooling (TOA DARE < 0), depending on the aerosol properties and the lower boundary condition (i.e., underlying cloud reflectance for the present application). This principle is evident in Figure 11, which shows mean above-cloud DARE, calculated from the pixel-level smoke subtype only broadband RT calculations used in Figure 10 (again, using the bias-adjusted cloud optical properties), as a function of both above-cloud AOD and underlying COT. Here as expected, the magnitude of DARE decreases as AOD decreases. However, DARE also decreases as the underlying clouds darken (i.e., as COT decreases), ultimately turning negative when COT is sufficiently small (for the smoke subtype analysis, this COT threshold is roughly between 2 and 4, depending on the overlying AOD). This behavior was also observed in the analyses of *Keil and Haywood* [2003] and *Chand et al.* [2009], who found that DARE became negative when the underlying cloud fraction fell below 56% and 40%, respectively.

[39] Figure 12 shows meridional averages of the instantaneous TOA DARE for cloudy MODIS pixels with reliable CALIOP above-cloud smoke (Figure 12a) or smoke and polluted dust (Figure 12b) subtype aerosol retrievals (i.e., only polluted cloudy pixels). Here the solid and dashed lines denote DARE calculated using the aerosol-adjusted and non-adjusted MODIS cloud optical property retrievals, respectively; black and gray lines denote the use of the standard CALIOP-derived above-cloud AOD and the scaled AOD (to adjust for daytime CALIOP AOD biases, see section 2.1), respectively. It is clear that adjusting the MODIS cloud retrievals to account for the above-cloud NIR attenuation can significantly affect radiative effect calculations. Indeed, using the nonadjusted cloud retrievals yields mean instantaneous TOA DARE for the entire region of $6.6Wm^{-2}$ and $6.7Wm^{-2}$ for the smoke and smoke/dust unscaled AOD, respectively, while using the bias-adjusted cloud retrievals yields $9.2Wm^{-2}$ and $8.6Wm^{-2}$, respectively, a roughly 50% increase for each case. Scaling the CALIOP-derived AOD to empirically rectify the low-biased daytime retrievals (gray lines) intuitively increases TOA DARE relative to that calculated from the unscaled AOD (means of $14.9Wm^{-2}$ and $13.7Wm^{-2}$ for the smoke and smoke/dust cases, respectively); this is partly due not only to the increased AOD, but also to even larger COT resulting from a larger bias adjustment.

[40] The meridional averages of the instantaneous TOA RFE for polluted cloudy MODIS pixels are shown in Figure 12c. Again, the solid and dashed lines denote calculations using the aerosol adjusted and nonadjusted MODIS cloud optical property retrievals, respectively. Black and gray lines, however, denote the use of the CALIOP smoke AOD and the combined smoke/polluted dust AOD, respectively; because RFE is normalized by AOD, scaling the AOD by 1.5 yields only minimal differences. Similar to the DARE calculations, using the bias-adjusted cloud optical property retrievals increases the TOA RFE for both the smoke case ($50.9Wm^{-2}AOD^{-1}$ to $65.1Wm^{-2}AOD^{-1}$) and combined smoke/polluted dust case ($59.5Wm^{-2}AOD^{-1}$ to $71.2Wm^{-2}AOD^{-1}$). Note also that the combined smoke/polluted dust cases have larger RFE than their respective smoke-only cases, underscoring the importance of AOD spatial sampling.

[41] A summary of the regional scalar statistics (mean and standard deviation, σ) of the DARE calculations shown in Figure 12, as well as DARE averaged over all ocean-only water clouds (both clean and polluted), is provided in Table 2. Similar to the polluted cloudy DARE calculations, the mean DARE averaged over all clouds increases when using bias-adjusted cloud retrievals; the effects of changes in horizontal sampling due to the inclusion of the polluted dust subtype, however, is much more evident. In fact, the additional sampling (there is roughly a 150% increase in polluted cloudy pixels when including the polluted dust subtype) increases the mean all-cloud DARE by roughly 120 to 160% compared to the smoke subtype only calculations, or about $1Wm^{-2}$ for the case using bias adjustments to both the cloud retrievals and AOD.

[42] Also shown in Table 2 is the difference between the TOA DARE with and without the underlying clouds, $<\Delta DARE>$, defined as

$$< \Delta DARE >= DARE_{cloudy} - DARE_{clear} \quad (3)$$

where $DARE_{cloudy}$ is defined by equation (1). $DARE_{clear}$, the TOA DARE without the underlying clouds, is defined as

$$DARE_{clear} = F^{\uparrow}_{clear} - F^{\uparrow}_{aerosol} \quad (4)$$

where $F^{\uparrow}_{clear}$ and $F^{\uparrow}_{aerosol}$ are the upwelling TOA SW fluxes for pristine sky and cloudless sky with absorbing aerosols, respectively. The quantity $<\Delta DARE>$ defined in equation (3) can be considered as the impact of clouds on the radiative effect of the overlying aerosols. This impact is larger when using the bias-adjusted MODIS cloud retrievals (means of

19.5Wm^{-2} and 17.2Wm^{-2} for the smoke and smoke/dust AOD, respectively) rather than the unadjusted cloud retrievals (means of 16.8Wm^{-2} and 15.3Wm^{-2} for the smoke and smoke/dust AOD, respectively), although the relative differences in <ΔDARE> are much smaller than the polluted cloudy DARE differences (the absolute differences are roughly the same). Larger impacts are also evident using the scaled AOD (means of 29.9Wm^{-2} and 26.5Wm^{-2} for the smoke and smoke/dust cases, respectively); here the relative differences in <ΔDARE> due to AOD scaling are similar to the polluted cloudy DARE differences.

[43] Similar to previous investigations [e.g., *Keil and Haywood*, 2003; *Chand et al*., 2009], the present analysis shows that the TOA DARE of absorbing aerosols overlying MBL stratocumulus clouds is strongly dependent on the underlying cloud properties. This result is not insignificant, particularly given that remote sensing retrievals of the underlying cloud optical properties themselves can be significantly biased by the above-cloud aerosol absorption. Indeed, adjusting the cloud retrievals to account for this bias can change the instantaneous TOA DARE of a cloudy scene with overlying absorbing aerosols by at least 2Wm^{-2}, as shown in Figure 12 and Table 2. Similarly, increasing the AOD by 50% (i.e., scaled by 1.5 to account for the daytime CALIOP retrieval biases) yields DARE that is roughly up to 5Wm^{-2} larger. Moreover, Table 2 shows that for this region and season, the presence of underlying MBL stratocumulus clouds results in a change in DARE relative to clear skies (i.e., <ΔDARE>) roughly a factor of two larger than the polluted cloudy DARE, a finding consistent with the case study analysis of *Keil and Haywood* [2003]. Horizontal sampling of the aerosol layer is also a significant issue, particularly when averaging DARE over all (polluted and unpolluted) liquid phase cloudy pixels. These results all have important implications, as they underscore the need for accurate, unbiased representations of the spatial and temporal morphologies and optical properties of both the aerosol and underlying cloud layers.

[44] Finally, it is worth emphasizing once more that the results shown here are for instantaneous (at time of observation) calculations. Because the Aqua overpass is near local noon, these instantaneous values are likely substantially larger than daytime-averaged values of DARE. Performing such diurnal calculations would have been ill advised however, primarily because properly accounting for the solar zenith angle dependence of coupled cloud-aerosol radiative transfer requires information about the diurnal change of cloud and aerosol properties, or a priori assumptions regarding their diurnal variations (note that previous studies such as *Chand et al*. [2009] and *Wilcox* [2011] assume that cloud properties remain constant). As such, they are beyond the scope of this investigation, although they do merit further exploration in future efforts.

6. Discussion and Conclusions

[45] Absorbing aerosols, such as biomass burning smoke, strongly absorb radiation at visible/near-infrared (VIS/NIR) wavelengths, and their presence above low-altitude clouds can introduce biases in passive cloud optical property retrievals that use VIS/NIR channels (e.g., 0.86 μm over ocean surfaces) to infer cloud optical thickness (COT). Here we provide estimates of the biases in MODIS liquid cloud optical property retrievals (MOD06) resulting from above-cloud absorbing aerosol extinction, and determine the impacts of these biases on estimates of the above-cloud direct aerosol radiative effect (DARE). We focus particularly on the southeast Atlantic Ocean during austral winter (August/September 2006–2011), when an extensive biomass burning smoke layer advected from southern Africa overlies widespread marine boundary layer (MBL) clouds. Modifying MOD06 reflectance look-up tables (LUTs) to account for above-cloud absorbing aerosol attenuation increases the retrieved regional mean COT, averaged over this region and season for polluted MBL clouds only (Table 1) and all MBL clouds (Figure 4), by roughly 18% and 6%, respectively (the regional mean retrieved cloud effective radius, r_e, increases by roughly 11% and 2.6%, respectively, due to COT changes in the non-orthogonal LUTs used for the retrievals). Consequently, the magnitude of above-cloud instantaneous (near local noon for Aqua overpass) DARE also increases. For above-cloud aerosols identified by CALIOP as smoke, mean DARE in the study region increases from 6.6Wm^{-2} using the original MOD06 cloud retrievals to 9.2Wm^{-2} using the new cloud retrievals. The mean radiative impact of the underlying clouds on the radiative effect of the overlying absorbing aerosols relative to clear sky, <ΔDARE>, also increases from 16.8Wm^{-2} using the original cloud retrievals to 19.5Wm^{-2} using the new cloud retrievals.

[46] It is important to place these estimated cloud optical property and DARE differences in context with aggregated retrieval uncertainties. Beginning with Collection 5, baseline pixel-level uncertainty estimates for both COT and r_e are provided in MOD06. These uncertainties account for three error sources, namely, surface spectral albedo, combined instrument calibration and 1-D forward model errors, and above-cloud water vapor absorption [*Platnick et al*., 2004]. Uncertainty estimates for instantaneous AOD retrievals, accounting for SNR within a layer, instrument calibration, and accuracy of the lidar ratio, are likewise provided in the Version 3 CALIOP Aerosol Layer Product [*Young*, 2010]. Note that all error components of the COT, r_e, and AOD uncertainty estimates are considered to be random and uncorrelated, and therefore yield no biases after a sufficient spatial and temporal aggregation of pixels. For the region and season of interest, mean daily relative COT and r_e random uncertainties, averaged over all MODIS individual liquid phase cloud retrievals collocated with the CALIPSO ground track, are approximately 11% and 14%, respectively; mean daily relative above-cloud AOD random uncertainty is approximately 40%. Not accounting for above-cloud absorbing aerosol extinction causes systematic biases in the retrieved cloud properties. Again, from Table 1, accounting for these aerosols increases the mean liquid COT and r_e of polluted cloudy scenes by approximately 18% and 11%, respectively; using the CALIOP AOD adjusted for the day/night bias (i.e., daytime AOD increased by 50% to address CALIOP sampling issues due to reduced daytime signal-to-noise ratio, SNR), the mean COT and r_e increase by approximately 37% and 17%, respectively. While these retrieval biases are roughly on par with the daily mean random uncertainties, spatial and temporal aggregation decreases the random component roughly by the inverse of the square root of the number of days used in the analysis (assuming

individual error sources are uncorrelated from day to day, and the number of pixels and mean values for each day are approximately equivalent). The bias will therefore dominate the aggregated root mean square (RMS) uncertainty (combination of bias and random uncertainty). The COT biases, particularly when using CALIOP AOD adjusted for the day/night bias, are substantially larger than the respective mean daily random uncertainty and so will dominate even more.

[47] Furthermore, note that as discussed in section 5, DARE is essentially a function of AOD, COT, and r_e. Since the aggregated COT and r_e RMS uncertainties are dominated by the biases due to above-cloud aerosol extinction, they are both effectively a function of the aggregated RMS uncertainty of the CALIOP AOD, which itself will be dominated by the bias component. Thus, the dominant component to the temporally and spatially aggregated RMS uncertainty of COT, r_e, or DARE is expected to be the CALIOP AOD bias which, assuming it is on the order of the day/night bias discussed in section 2.1, has been detailed in Tables 1 and 2 and elsewhere. If however the CALIOP AOD bias is even larger than assumed here, as other results suggest (H. Jethva, personal communication), our DARE and $<\Delta$DARE$>$ estimates after AOD adjustment ($14.9\mathrm{Wm}^{-2}$ and $29.9\mathrm{Wm}^{-2}$, respectively, for smoke subtype aerosols) should be considered lower bounds.

[48] Yet an additional caveat remains in our analysis. Spatial sampling, limited here to the CALIPSO ground track, may also be limited by the MOD06 algorithm (e.g., partial retrievals or cloud edge pixels) and by the aforementioned low daytime CALIOP SNR, which can decrease CALIOP's sensitivity to optically thin aerosol layers (as well as to the full extent of the geometrical thickness of the aerosol layer) and potentially result in undetected aerosol layers or aerosol type misclassification. To expand the horizontal sampling, we included the polluted dust aerosol subtype as a smoke aerosol in the analysis, and found slight decreases in the COT and r_e adjustments, DARE, and $<\Delta$DARE$>$ compared to those using only the smoke aerosol subtype. Regardless of these caveats, it is clear that CALIOP provides a valuable resource for investigating above-cloud aerosols given its ability to detect and retrieve optically thin atmospheric features.

[49] A logical next step would be to expand the instantaneous, time of observation DARE calculations shown here to provide estimates of daily averaged DARE, an exercise, however, that would introduce considerable uncertainty in the DARE calculations due to the unknown diurnal variation in cloud and aerosol properties. In addition, exploiting the full sampling potential of MODIS by expanding the analysis to full swath is of great interest; note that recent work has shown promise toward obtaining full swath above-cloud absorbing aerosol retrievals using OMI [*Torres et al.*, 2012] and MODIS [*Jethva et al.*, 2013]. But ultimately, this is another example of why A-Train intersensor synergy has been, and will continue to be, important for expanding the current knowledge of aerosols and their radiative effects.

[50] **Acknowledgments.** The authors would like to thank Nandana Amarasinghe for his efforts to construct the cloud retrieval look-up tables and Gala Wind for her extensive work on the development of the MOD06 Collection 6 algorithm. In addition, the authors wish to thank Zhibo Zhang for his generous intellectual support during the course of this work and Rob Levy for his assistance with the aerosol component. The MODIS data used in this study were acquired as part of the NASA's Earth-Sun System Division and archived and distributed by the MODIS Adaptive Processing System (MODAPS); CALIOP data were obtained from the NASA Langley Research Center Atmospheric Science Data Center. This research was supported by the NASA Radiation Sciences Program.

References

Ackerman, A. S., M. P. Kirkpatrick, D. E. Stevens, and O. B. Toon (2004), The impact of humidity above stratiform clouds on indirect aerosol climate forcing, *Nature*, *432*, 1014–1017.

Albrecht, B. A. (1989), Aerosols, cloud microphysics, and fractional cloudiness, *Science*, *245*, 1227–1230.

Bond, T. C., and R. W. Bergstrom (2006), Light absorption by carbonaceous particles: An investigative review, *Aerosol Sci. Technol.*, *40*, 27–67.

Chand, D., T. L. Anderson, R. Wood, R. J. Charlson, Y. Hu, Z. Liu, and M. Vaughan (2008), Quantifying above-cloud aerosol using spaceborne lidar for improved understanding of cloudy-sky direct climate forcing, *J. Geophys. Res.*, *113*, D13206, doi:10.1029/2007JD009433.

Chand, D., R. Wood, T. L. Anderson, S. K. Satheesh, and R. J. Charlson (2009), Satellite-derived direct radiative effect of aerosols dependent on cloud cover, *Nat. Geosci.*, *2*, 181–184.

Clough, S. A., M. W. Shephard, E. J. Mlawer, J. S. Delamere, M. J. Iacono, K. Cady-Pereira, S. Boukabara, and P. D. Brown (2005), Atmospheric radiative transfer modeling: A summary of the AER codes, *J. Quant. Spectrosc. Radiat. Transfer*, *91*, 233–244.

Cox, C., and W. Munk (1954a), Measurements of the roughness of the sea surface from photographs of the Sun's glitter, *J. Opt. Soc. Am.*, *44*, 838–850.

Cox, C., and W. Munk (1954b), Statistics of the sea surface derived from Sun glitter, *J. Mar. Res.*, *13*, 198–227.

Derber, J. C., D. F. Parrish, and S. J. Lord (1991), The new global operational analysis system at the National Meteorological Center, *Weath. Forec.*, *6*, 538–547.

Devasthale, A., and M. A. Thomas (2011), A global survey of aerosol-liquid water cloud overlap based on four years of CALIPSO-CALIOP data, *Atmos. Chem. Phys.*, *11*, 1143–1154, doi:10.5194/acp-11-1143-2011.

de Graaf, M., L. G. Tilstra, P. Wang, and P. Stammes (2012), Retrieval of the aerosol direct radiative effect over clouds from spaceborne spectrometry, *J. Geophys. Res.*, *117*, D07207, doi:10.1029/2011JD017160.

Eck, T. F., et al. (2003), Variability of biomass burning aerosol optical characteristics in southern Africa during the SAFARI 2000 dry season campaign and a comparison of single scattering albedo estimates from radiometric measurements, *J. Geophys. Res.*, *108*(D13), 8477, doi:10.1029/2002JD002321.

Forster, P., et al. (2007), Changes in atmospheric constituents and in radiative forcing, in *Climate Change 2007: The Physical Science Basis. Contribution of Working Group I to the Fourth Assessment Report of the Intergovernmental Panel on Climate Change* edited by S. Solomon, D. Qin, M. Manning, Z. Chen, M. Marquis, K. B. Averyt, M. Tignor and H. L. Miller, Cambridge University Press, Cambridge.

Haywood, J. M., S. R. Osborne, and S. J. Abel (2004), The effect of overlying absorbing aerosol layers on remote sensing retrievals of cloud effective radius and cloud optical depth, *Q. J. R. Meteorol. Soc.*, *130*, 779–800.

Holz, R. E., S. A. Ackerman, F. W. Nagle, R. Frey, S. Dutcher, R. E. Kuehn, M. A. Vaughan, and B. Baum (2008), Global Moderate Resolution Imaging Spectroradiometer (MODIS) cloud detection and height evaluation using CALIOP, *J. Geophys. Res.*, *113*, D00A19, doi:10.1029/2008JD009837.

Hu, Y., M. Vaughan, Z. Liu, K. Powell, and S. Rodier (2007), Retrieving optical depths and lidar ratios for transparent layers above opaque water clouds from CALIPSO lidar measurements. IEEE *Geosci. Remote Sens. Lett.*, *4*, 523-526.

Hu, Y., et al. (2009), CALIPSO/CALIOP cloud phase discrimination algorithm, *J. Atmos. Oceanic Technol.*, *26*, 2293–2309, doi:10.1175/2009JTECHA1280.1.

Iacono, M. J., J. S. Delamere, E. J. Mlawer, M. W. Shephard, S. A. Clough, and W. D. Collins (2008), Radiative forcing by long-lived greenhouse gases: Calculations with the AER radiative transfer models, *J. Geophys. Res.*, *113*, D13103, doi:10.1029/2008JD009944.

Joseph, J. H., W. J. Wiscombe, and J. A. Weinman (1976), The delta-Eddington approximation for radiative flux transfer, *J. Atmos. Sci.*, *33*, 2452–2459.

Jethva, H., O. Torres, L. A. Remer, and P. K. Bhartia (2013), A color ratio method for simultaneous retrieval of aerosol and cloud optical thickness of above-cloud absorbing aerosols from passive sensors: Application to MODIS measurements. *IEEE Trans. Geosci. Remote Sens.*, doi:10.1109/TGRS.2012.2230008.

Keil, A., and J. M. Haywood (2003), Solar radiative forcing by biomass burning aerosol particles during SAFARI 2000: A case study based on measured aerosol and cloud properties, *J. Geophys. Res.*, *108*(D13), 8467, doi:10.1029/2002JD002315.

King, M. D., S.-C. Tsay, S. E. Platnick, M. Wang, and K.-N. Liou (1998), Cloud retrieval algorithms for MODIS: Optical thickness, effective particle radius, and thermodynamic phase. Products: 06_L2 (OD). ATBD Reference Number: ATBD-MOD-05.

Levy, R. C., L. A. Remer, D. Tanre, S. Mattoo, and Y. J. Kaufman (2009), Algorithm for remote sensing of tropospheric aerosol over dark targets from MODIS. ATBD Reference Number: ATBD-MOD-04.

Liu, Z., M. A. Vaughan, D. M. Winker, C. A. Hostetler, L. R. Poole, D. L. Hlavka, W. D. Hart, and M. J. McGill (2004), Use of probability distribution functions for discriminating between cloud and aerosol in lidar backscatter data, *J. Geophys. Res.*, *109*, D15202, doi:10.1029/2004JD004732.

Liu, Z., M. A. Vaughan, D. M. Winker, C. Kittaka, R. E. Kuehn, B. J. Getzewich, C. R. Trepte, and C. A. Hostetler (2009), The CALIPSO lidar cloud and aerosol discrimination: Version 2 algorithm and initial assessment of performance, *J. Atmos. Oceanic Technol.*, *26*, 1198–1213, doi:10.1175/2009JTECHA1229.1.

Matichuk, R. I., P. R. Colarco, J. A. Smith, and O. B. Toon (2006), Modeling the transport and optical properties of smoke aerosols from African savanna fires during the Southern African Regional Science Initiative campaign (SAFARI 2000), *J. Geophys. Res.*, *112*, D08203, doi:10.1029/2006JD007528.

Meador, W. E., and W. R. Weaver (1980), Two-stream approximations to radiative transfer in planetary atmospheres: A unified description of existing methods and a new improvement, *J. Atmos. Sci.*, *37*, 630–643.

Nakajima, T., and M. D. King (1990), Determination of the optical thickness and effective particle radius of clouds from reflected solar radiation measurements part I: Theory, *J. Atmos. Sci.*, *47*, 1878–1893.

Omar, A. H., J.-G. Won, D. M. Winker, S.-C. Yoon, O. Dubovik, and M. P. McCormick (2005), Development of global aerosol models using cluster analysis of Aerosol Robotic Network (AERONET) measurements, *J. Geophys. Res.*, *110*, D10S14, doi:10.1029/2004JD004874.

Omar, A., et al. (2009), The CALIPSO automated aerosol classification and lidar ratio selection algorithm, *J. Atmos. Oceanic Technol.*, *26*, 1994–2014, doi:10.1175/2009JTECHA1231.1.

Oreopoulos, L., and H. W. Barker (1999), Accounting for subgrid-scale cloud variability in a multi-layer 1-D solar radiative transfer algorithm, *Q. J. R. Meteorolog. Soc.*, *125*, 301–330.

Pincus, R., S. Platnick, S. A. Ackerman, R. S. Hemler, and R. J. P. Hofmann (2012), Reconciling simulated and observed views of clouds: MODIS, ISCCP, and the limits of instrument simulators, *J. Climate*, *25*, 4699–4720.

Platnick, S., and S. Twomey (1994), Determining the susceptibility of cloud albedo to changes in droplet concentration with the Advanced Very High Resolution Radiometer, *J. Appl. Meteorol.*, *33*, 334–347.

Platnick, S., M. D. King, S. A. Ackerman, W. P. Menzel, B. A. Baum, J. C. Riedi, and R. A. Frey (2003), The MODIS cloud products: Algorithms and examples from Terra, *IEEE Trans. Geosci. Remote Sens.*, *41*, 459–473.

Platnick, S., R. Pincus, B. Wind, M. D. King, M. Gray, and P. Hubanks (2004), An initial analysis of the pixel-level uncertainties in global MODIS cloud optical thickness and effective particle size retrievals, *Passive Opt. Remote Sens. Atmos. Clouds IV, Proc. of SPIE*, *5652*, doi:10.1117/12.578353.

Stamnes, K., S.-C. Tsay, W. Wiscombe, and K. Jayaweera (1988), A numerically stable algorithm for discrete-ordinate-method radiative transfer in multiple scattering and emitting layered media, *Appl. Opt.*, *27*, 2502–2509.

Torres, O., H. Jethva, and P. K. Bhartia (2012), Retrieval of aerosol optical depth above clouds from OMI observations: Sensitivity analysis and case studies, *J. Atmos. Sci.*, *69*, 1037–1053.

Twomey, S. (1974), Pollution and the planetary albedo, *Atmos. Environ.*, *8*, 1251–1256.

Twomey, S. (1977a), The influence of pollution on the shortwave albedo of clouds, *J. Atmos. Sci.*, *34*, 1149–1152.

Twomey, S. (1977b), *Atmospheric Aerosols, Section 12.3*, pp. 278-290, Elsevier Scientific Publishing Co., United Kingdom.

van der Werf, G. R., J. T. Randerson, L. Giglio, G. J. Collatz, M. Mu, P. S. Kasibhatla, D. C. Morton, R. S. DeFries, Y. Jin, and T. T. van Leeuwen (2010), Global fire emissions and the contribution of deforestation, savanna, forest, agriculture, and peat fires (1997–2009), *Atmos. Chem. Phys.*, *10*, 11707–11735, doi:10.5194/acp-10-11707-2010.

Vaughan, M. A., K. A. Powell, D. M. Winker, C. A. Hostetler, R. E. Kuehn, W. H. Hunt, B. J. Getzewich, S. A. Young, Z. Liu, and M. J. McGill (2009), Fully automated detection of cloud and aerosol layers in the CALIPSO lidar measurements, *J. Atmos. Oceanic Technol.*, *26*, 2034–2050, doi:10.1175/2009JTECHA1228.1.

Wilcox, E. M., Harshvardhan, and S. Platnick (2009), Estimate of the impact of absorbing aerosol over cloud on the MODIS retrievals of cloud optical thickness and effective radius using two independent retrievals of liquid water path, *J. Geophys. Res.*, *114*, D20215, doi:10.1029/2008JD010589.

Wilcox, E. M. (2011), Direct and semi-direct radiative forcing of smoke aerosols over clouds, *Atmos. Chem. Phys. Discuss.*, *11*, doi:10.5194/acpd-11-20947-2011.

Winker, D. M., M. A. Vaughan, A. H. Omar, Y. Hu, K. A. Powell, Z. Liu, W. H. Hunt, and S. A. Young (2009), Overview of the CALIPSO mission and CALIOP data processing algorithms, *J. Atmos. Oceanic Technol.*, *26*, 2310–2323, doi:10.1175/2009JTECHA1281.1.

Winker, D. M., J. L. Tackett, B. J. Getzewich, Z. Liu, M. A. Vaughan, and R. R. Rogers (2012), The global 3-D distribution of tropospheric aerosols as characterized by CALIOP, *Atmos. Chem. Phys. Discuss.*, *12*, 24847–24893.

Wiscombe, W. (1980), Improved Mie scattering algorithms, *Appl. Opt.*, *19*, 1505–1509.

Young, S. A., and M. A. Vaughan (2009), The retrieval of profiles of particulate extinction from Cloud Aerosol Lidar and Pathfinder Satellite Observations (CALIPSO) data: Algorithm description, *J. Atmos. Oceanic Technol.*, *26*, 1105–1119, doi:10.1175/2008JTECHA1221.1.

Young, S. (2010), Uncertainty analysis for particulate backscatter, extinction and optical depth retrievals reported in the CALIPSO Level 2, Version 3 data release. CALIPSO Version 3 Extinction Uncertainty Document.

Zhang, Z., and S. Platnick (2011), An assessment of differences between cloud effective particle radius retrievals for marine water clouds from three MODIS spectral bands, *J. Geophys. Res.*, *116*, D20215, doi:10.1029/2011JD016216.